



Research on element migration and ash deposition characteristics of high-alkali coal in horizontal liquid slagging cyclone furnace

Shihao Hu, Yuguo Ni, Qi Yin, Jiankang Wang, Laiquan Lv, Kefa Cen, Hao Zhou *

Zhejiang University, Institute for Thermal Power Engineering, State Key Laboratory of Clean Energy Utilization, Hangzhou 310027, PR China

ARTICLE INFO

Keywords:

High-alkali coal
Liquid slagging cyclone furnace
Element migration
Deposition characteristics
Crystal structure

ABSTRACT

Hongshaquan coal (HSQ), a kind of high-alkali and rich-iron coal, is burned in a 20 MW liquid slagging cyclone furnace. The migration and transformation characteristics of elements are examined. The deposition probe and oil cooling circulation system are used to investigate the ash deposition characteristics of HSQ. In addition, the microscopic morphology, crystal structure and chemical composition of the slag are studied to explain the effect of element migration on ash deposition and slag. The results show that the growth process of deposition on probe 1 can be divided into four stages. The final stable relative heat flux of probe 1 and probe 2 is 0.585 and 0.85, respectively. The average concentration of Na_2O in ash is 4.53%. Na, K, Ca, Mg and S are enriched in the low temperature area of the boiler to form sulfate which leads to the agglomeration of ash particles. The main mineral phases of the slag are silicates and iron-containing compounds. The average concentration of Fe_2O_3 in the slag sample is 36.73%. Iron will be enriched in the slag and form a low-temperature eutectic with the silicon-calcium-magnesium-aluminum system to reduce the melting point of the ash. The granulated slag has a lower degree of crystallinity and is closer to the characteristics of glassy slag, which is due to the low content of Na_2O , CaO and high silicon-to-aluminum ratio in the ash.

1. Introduction

As the main form of energy utilization in China, coal combustion accounts for more than 50% of primary energy consumption [1,2]. Zhundong coalfield, located in Changji Hui Autonomous Prefecture, Xinjiang Province, contains 390 billion tons of coal in the narrow and long area 220 km from east to west, which is the largest integrated coal field in China [3,4]. Due to the advantages of large reserves, convenient mining and low ash content, Zhundong coal (ZDC) has attracted much attention from academia and industry. However, the content of alkali metals and alkaline earth metals in ZDC is higher than that in ordinary coal, which will lead to more serious slagging, fouling and corrosion of heat transfer surface [5,6]. These problems will increase the operational risk of coal-fired power plant, reduce the heat transfer efficiency of the boiler and increase the operation cost. Therefore, it is necessary to study the characteristics of element migration and slagging deposition on the heating surface in the combustion process of ZDC, which is conducive to the effective utilization of ZDC on an industrial scale.

The sodium element in coal mainly exists in four forms [7]: water-soluble sodium, ammonium acetate-soluble sodium, acid-soluble

sodium, and acid-insoluble sodium. Water soluble sodium is the primary occurrence form of sodium in ZDC. In the combustion process of ZDC, a large amount of sodium evaporates from the coal due to high temperature and then condenses on the low temperature heat exchange surface to form a sticky layer to capture ash particles [8]. Scholars have done a lot of research on the occurrence and migration of alkali metal sodium in ZDC. Li [9] et al. studied the influence of temperature between 400 °C and 1000 °C on sodium conversion behavior during ZDC combustion. The experimental results show that as the temperature increases, more sodium will decompose into the gas phase. Most of the sodium is released into the gas phase in the form of NaCl, and the remaining sodium is converted into aluminosilicate at high temperature. Sodium deposition mainly occurs above 873 K, and will react with the ash deposited on the heat transfer surface under high temperature (1073 K) conditions [10]. Liang [11] studied the alkali metal migration behavior during ZDC pyrolysis process. A part of water-soluble alkali metals will be released into the gas phase during pyrolysis, but the coke matrix has an inhibitory effect on the release of alkali metal compounds, so the alkali metals will be enriched on the surface of the char. Yu [12] studied the release and migration characteristics of sodium and potassium in

* Corresponding author.

E-mail address: zhouhao@zju.edu.cn (H. Zhou).

<https://doi.org/10.1016/j.fuel.2021.121962>

Received 1 August 2021; Received in revised form 30 August 2021; Accepted 7 September 2021

Available online 14 September 2021

0016-2361/© 2021 Elsevier Ltd. All rights reserved.

ZDC under an oxy-fuel combustion environment. The research found that the sodium content in the ash decreases as the oxygen concentration increases, while the potassium content increases in both air environment and oxy-fuel environment. Wang [13] and Xu [3] studied the effect of silicon aluminum additives on the migration of alkali metals in ZDC. Silicon-aluminum additives can significantly reduce the release of sodium. This is because the silicon-aluminum additive can promote the conversion of water-soluble sodium to insoluble form and can adsorb alkali metals to induce the formation of low-melting eutectic substances.

At present, the utilization of ZDC is mostly co-fired with conventional coal or converted into gas fuel in the gasifier. Chen [14] examined the relationship between the viscosity of the slag and the temperature with different Na_2O content under gasification conditions. In addition, the crystallization mechanism of slag was studied and a new evaluation standard of crystallization tendency was proposed. Zhou [15] studied the slagging and fouling characteristics of ZDC in a 300 kW solid slagging experimental furnace. The study found that the cross-section of the slag presents a three-layer structure, and the growth curve of the deposition thickness shows that the growth of the slag is divided into four stages. Song [16] analyzed the chemical composition, mineralogical composition and microstructure of the gasification slag. A high-temperature rheometer was used to measure the rheological properties, thixotropic behavior and yield stress of slag in the temperature range of 500 ~ 1550°C.

The liquid slagging cyclone furnace has the advantages of high combustion efficiency and less fly ash is considered to be effective equipment for the combustion of high-alkali ZDC. However, there are few researches on the combustion of ZDC in liquid slagging cyclone furnace. Furthermore, most of the researches on ZDC mainly focus on the occurrence and migration characteristics of alkali metals, especially sodium, while there are few reports on the other metals.

In the research described in this paper, Hongshaquan coal (HSQ), a kind of ZDC, is burned in a 20 MW liquid slagging cyclone furnace. The migration and transformation characteristics of elements are examined. The deposition probe and oil cooling circulation system are used to investigate the ash deposition characteristics of HSQ. In addition, the microscopic morphology, crystal structure and chemical composition of the slag are studied to explain the effect of element migration on ash deposition and slag.

2. Experimental and analytical methods

2.1. Combustion facility and coal characterization

The experiment is conducted in a 20 MW liquid slagging cyclone furnace system. As shown in Fig. 1, the experimental system is mainly composed of a horizontal cyclone furnace, a burnout chamber, a coal feeder, a swirl burner, a forced draft fan, an induced draft fan, a slag conveyor, a cooling pool and a deposition sampling system. The inner diameter and the length of the cyclone barrel are 1500 mm and 2240 mm, respectively. Thermocouples are installed in the cyclone and the burnout chamber to monitor the temperatures of various parts of the furnace. Two S-type thermocouples are symmetrically arranged in the cyclone. Six S-type thermocouples are arranged at the bottom of the burnout chamber, and four are arranged in the middle and upper part of the burnout chamber respectively. Two S-type thermocouples are respectively arranged on the upper and lower sides of the outlet of the burnout chamber. An insulation layer is installed on the outer wall of the furnace to reduce heat loss. Natural gas is employed for ignition in the experiment. The coal feeding is started with a rate of 2.3 t/h after the temperature of the furnace is stable. During the experiment, all secondary air inlets remain open, and the valve opening changes according to the air volume and velocity. The pulverized coal is carried by the primary air through the swirl burner axially into the cyclone barrel, and forms strong swirl combustion under the action of the high-speed tangential secondary air, which extends the residence time of pulverized coal particles in the cyclone barrel and produces a large amount of liquid slag. The high-temperature flue gas produced by the combustion of pulverized coal enters the burnout chamber through the outlet of the cyclone barrel. Due to the obstruction of the partition of the burnout chamber and the slag screen, the flue gas changes its direction twice in the burnout chamber. Most of the liquid slag in the flue gas hits the wall under the action of centrifugal force, thus forming the bottom slag, which is discharged from the slag hole at the bottom of the burnout chamber. Then the flue gas enters the air preheater through the outlet of the burnout chamber after cooling by the thermostat screen and heat transfer surface at the end of burnout chamber. The low temperature flue gas is discharged into the atmosphere from the chimney after dust removal and denitration. The experimental conditions are shown in Table 1. The feeding rate, primary air volume, secondary air volume,

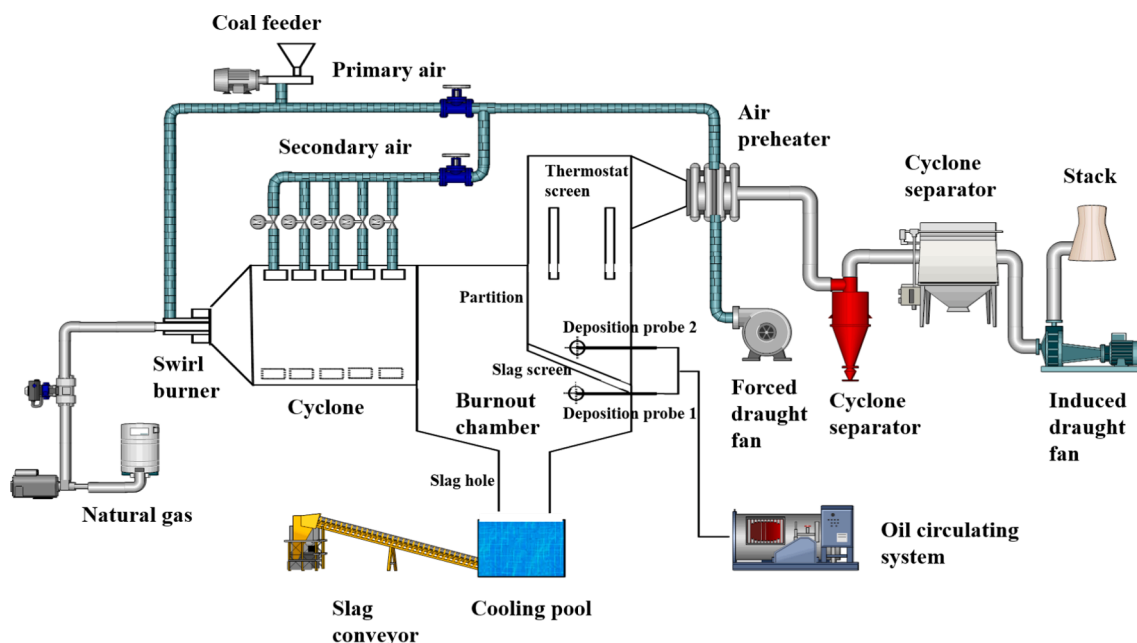


Fig. 1. The schematic diagram of the experimental system.

Table 1
Experimental parameter.

Coal sample	HSQ
Fuel feed rate (t/h)	2.3
Oxygen concentration at the furnace outlet (%)	4–5%
Excess air ratio	1.2
Primary air volume (Nm ³ /h)	2700
Secondary air volume (Nm ³ /h)	13,500
Primary air temperature (°C)	230
Secondary air temperature (°C)	250
Temperature of the cyclone (°C)	~1400
Temperature around deposition probe 1 (°C)	~1300
Temperature around deposition probe 2 (°C)	~1100

primary air temperature and secondary air temperature given in Table 1 are controlled by program and remain unchanged during the experiment. The parameters such as furnace temperature and oxygen concentration at the furnace outlet are the average values measured when the experiment is stable. As shown in Table 1, the volume of the primary air is 2700 Nm³/h, and the volume of the secondary air is 13,500 Nm³/h. This is because in the design of horizontal liquid slagging cyclone furnace, the primary air accounts for only about 15% of the total air volume, while the secondary air accounts for about 80%. The secondary air inlets are arranged tangentially on both sides of the cyclone, and the velocity is generally 50–55 m/s, so as to form a strong swirling flow in the furnace, enhance the disturbance, combustion intensity and slag separation.

The coal used in this experiment is Hongshaquan coal (HSQ). The proximate analysis, ultimate analysis, ash composition analysis and ash fusion temperature of HSQ are shown in Table 2. The content of Na₂O in the ash is as high as 3.18%, which indicates that HSQ belongs to high-alkali coal, and the content of Fe₂O₃ in the ash is also higher than conventional coal. The softening temperature (ST) of the ash is lower than 1260 °C, which is the characteristic of serious slagging coals.

Table 2
Coal properties

HSQ coal		
Proximate analysis (wt.%, ad)	M _t (wt.%) Total Moisture	22
	Moisture	14.63
	Ash	7.52
	Volatiles matter	32.82
Ultimate analysis (wt.%, ad)	Fixed carbon	45.03
	Carbon	61.52
	Hydrogen	3.59
	Oxygen	11.48
	Nitrogen	0.84
HV (MJ/kg)	Sulfur	0.42
	Q _{ad,gr}	24.308
Ash fusion temperature (°C)	DT	1096
	ST	1107
	HT	1109
	FT	1114
Ash composition (wt.%)	SiO ₂	31.52
	Al ₂ O ₃	13.32
	CaO	16.63
	Fe ₂ O ₃	18.68
	SO ₃	7.66
	MgO	6.19
	K ₂ O	0.89
	TiO ₂	0.95
	Na ₂ O	3.18
	P ₂ O ₅	0.30

2.2. Deposit sampling technology

When the combustion in the furnace is stable, a 2.3 m-long deposition probe is inserted into the front and back of the slag screen, respectively. The deposition part of the probe is 76 mm in length and 40 mm in outer diameter, and is connected to the oil-cooled pipeline through a thread, as shown in Fig. 2(I). Two radially distributed small holes are arranged at the cross-section of the probe deposition part, with an inner diameter of 1.8 mm and an interval of 4 mm, as shown in Fig. 2 (II). Two K-type thermocouples are installed in the small holes to monitor the temperatures of the inner and outer surfaces of the deposition part. The temperatures of the deposition probes are controlled by the oil circulation system (LEOT-30-24T-2). During the experiment, the temperature of the inner surface of the deposition probe is controlled around 340°C, and the probe inserting time under each condition is 60 min.

After the experiment completed, the furnace is cooled to the normal atmospheric temperature. The samples are collected to analyze the element migration characteristics of HSQ combustion in horizontal liquid slagging cyclone furnace from the following position: the partition of the burnout chamber, the slag hole, the windward side of slag screen, the cooling water tank, the heat transfer surface at the end of burnout chamber, the leeward side of slag screen and the thermostat screen.

2.3. Detection and analysis methods

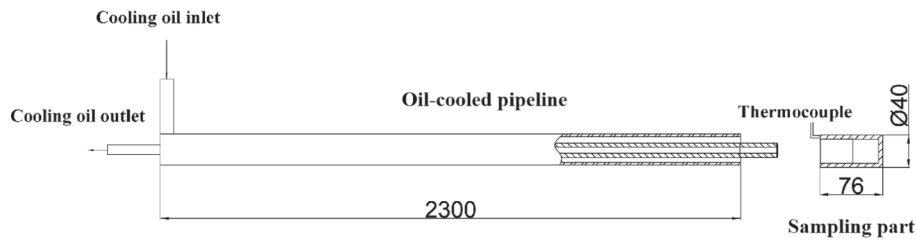
The growth of deposition concentrated on the windward side of the deposition part of the probe, so the heat transfer process of the deposition part can be simplified as a one-dimensional heat conduction process along the radial direction of the cylinder [17]. The heat flux through the deposition can be expressed as:

$$q = -\lambda \frac{dt}{dr} = \frac{\lambda(T_1 - T_2)}{R \ln\left(\frac{R_1}{R_2}\right)} \quad (1)$$

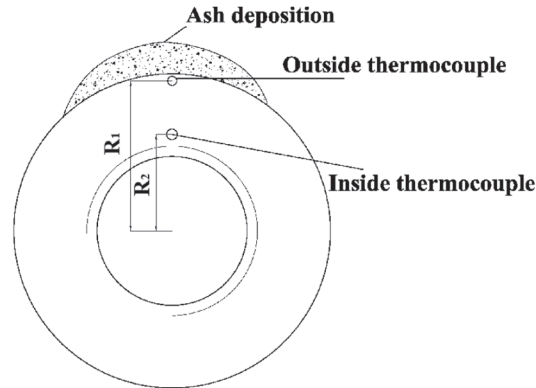
where λ indicates the thermal conductivity of the deposition part of the probe. T_1 and T_2 are the temperatures of the inner surface and the outer surface of the probe, respectively. R_1 and R_2 are the distances from the inner and outer holes of the probe to the center of the circle, respectively. R means the radius of the deposition part of the probe. In order to reflect the influence of deposition on the heat transfer of the heat exchange surface intuitively, the relative heat flux is calculated, which is defined as the ratio of heat flux to initial heat flux q_0 .

The slag and deposition samples collected from different parts of the furnace are placed in a special mold, then immersed with epoxy resin for more than 24 h. Hereafter, the slag samples wrapped in resin are cut and polished using the Struers cutting machine and Struers Tegrabo-35, respectively. The processed slag samples then are observed with a Zeiss Axioskop reflective metallographic microscope at 25 times magnification. A CCD camera connected to the microscope is used to record and transfer photos to the computer. The pictures taken by the CCD camera are processed by the software Axiovision to obtain the area of the mineral phases and pores, and the two-dimensional porosity of the slag samples can be calculated. The two-dimensional porosity can reflect the compactness of slag samples to a certain extent.

The microstructure of the slag and deposition samples are observed by a tungsten scanning electron microscope (Hitachi S-3700N), and the elemental composition is analyzed by Energy Dispersive X-Ray Spectroscopy (EDX). The slag and deposition samples are tested by X-ray diffractometer (PANalytical B.V. X-pert Powder) to analyze the mineral composition after ground into particles below 45 μ m. The oxide and elemental composition of the samples are detected by X-Ray Fluorescence (XRF, Shimadzu xrf-1800).



(I) The deposition probe



(II) The cross-section of the sampling part

Fig. 2. Schematic of deposition probe.

3. Results and discussion

3.1. Visual evaluation of slag and deposition

Fig. 3 shows the appearance of slag and deposition samples at different positions in the furnace. The slag sample at the partition of the burnout chamber (⊙) has a high density and smooth surface. According to the color and structure of the cross-section, the slag sample can be divided into three layers: The bottom layer is dense and the color is dark black; the middle layer has the largest thickness, gray-black with many bubbles; the top layer is bright black with dense small pore bubbles. There are obvious flow marks on the surface of the slag sample at the slag hole (⊗). The cross-section of the slag can be divided into two layers, the upper layer is bright black, and the bottom layer is gray-black. The slag sample on the windward side of the slag screen (⊙) is gray-black as a whole. The slag can be divided into two layers. The obvious shape of droplets can be seen in the bottom layer, which is formed by the impact of liquid slag on the slag screen; the slag droplets in the upper layer merge with each other to form a relatively smooth surface, but there are still unclosed pores. The granulated slag in cooling water tank (⊙) is black with obvious glass luster and light weight. With the decrease of flue gas temperature, the ash collected in the low temperature region of the burnout chamber does not become a molten state, and adheres to the heat exchange surface in the form of ash fouling. The ash collected from the leeward side of the slag screen (⊙) and the thermostat screen (⊙) in khaki, while the ash collected from the heat transfer surface at the end of burnout chamber (⊙) is gray.

Fig. 4 shows the deposition collected by the deposition probe. (a) Is the slag sample collected on the windward side of probe 1. Which can be completely removed from the probe. Similar to the slag collected on the windward side of the slag screen, it is formed by the fusion of the liquid slag impinging on the surface of the probe, so there are obvious drop shapes and gaps at the bottom of the deposition. In addition, the pore structure can be obviously observed on the surface of the deposition. The

deposition on the leeward side of probe 1 is khaki with loose adhesion, as shown in Fig. 4(b), which can be easily scraped off with a knife. (c) It is the deposition on the windward surface of probe 2, which is dense gray-black sediment with hard solid particles dotted on its surface. The deposition is closely attached to the probe surface and is difficult to scrape off. (d) Is the deposition on the leeward side of probe 2, with loose khaki ash at the bottom and dark brown small particles cover on the upper.

3.2. Heat flux through the deposition

Fig. 5 shows the temperatures distribution near the probes during the experiment. It can be seen from the figure that the temperature around probe 1 is about 1300 °C and the temperature around probe 2 is about 1100 °C. The average deviation is 3.61% and 4.25% respectively. Therefore, it is reasonable to believe that the temperatures around deposition probes remains unchanged during the experiment.

Fig. 6 delineates the variation of heat flux through probes with time. The curve of probe 1 can be divided into four stages, according to the change rate of heat flux. Stage 1 is the rapid decline stage (OA), stage 2 is the slow descent stage (AB), stage 3 is the re-descent stage (BC), and stage 4 is the stable stage (CD). The durations of each stage are 18, 13, 15 and 14 min, while the decline rates are 0.0147, 0.00208, 0.0082 and 0 (1/min), respectively. The heat flux of the probe 1 decreases rapidly in the OA stage, which indicates that the thermal resistance of the initial layer is large. This phenomenon is due to the fact that in the initial stage of deposition, the granular liquid slag is entrained by hot flue gas and impacts on the surface of the low temperature probe. The liquid slag adheres to the surface of the probe and solidifies rapidly. The large gap between the solidified spherical slag results in a small thermal conductivity. The obvious pore structure observed in the bottom of the deposition described in Section 3.1 and the difference in porosity between the upper and bottom layers in Section 3.3 can support this inference. With the formation of the initial layer, the temperature of the deposit surface

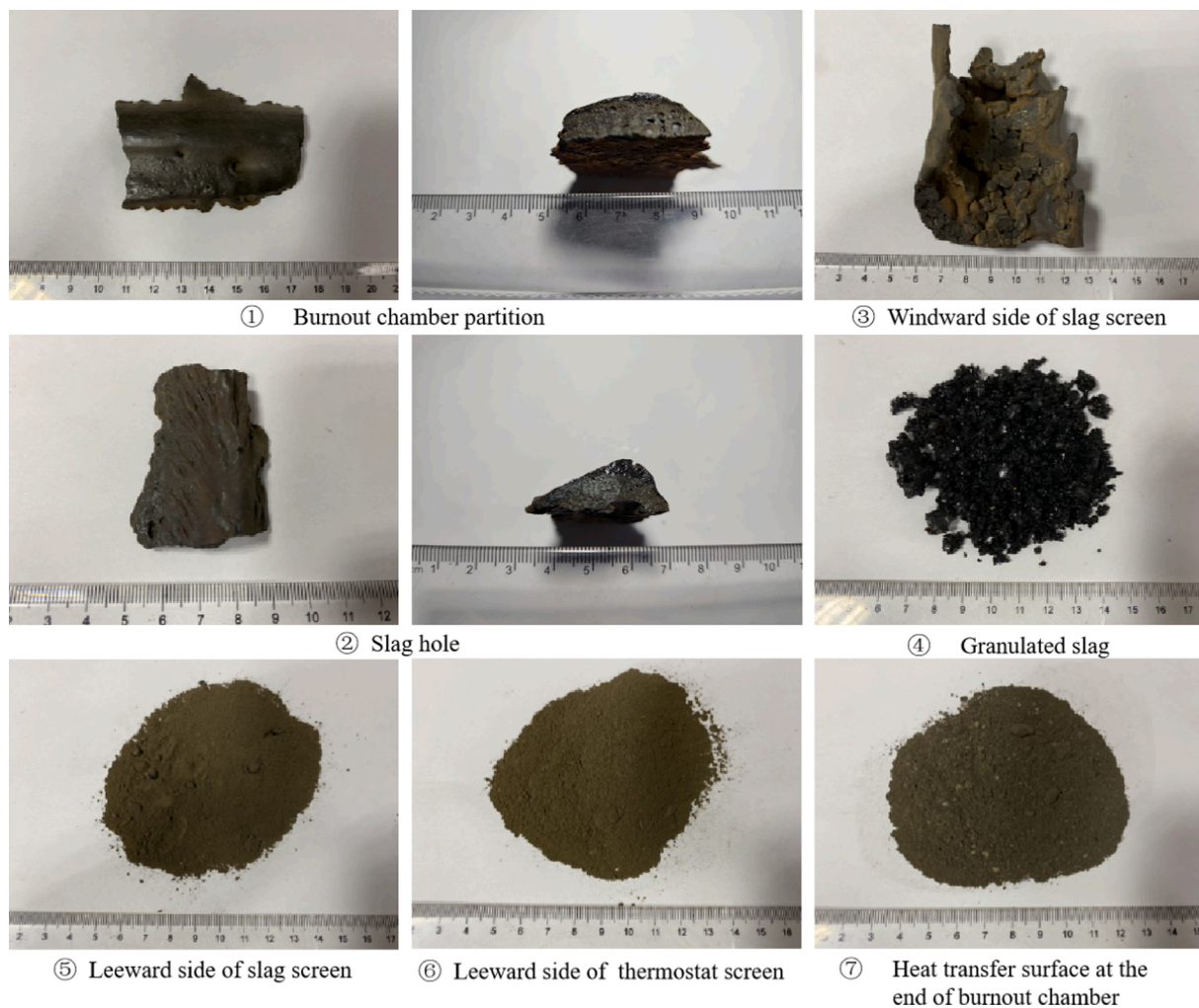


Fig. 3. The appearance of slag and ash at different positions in the furnace.

is much higher than that of the probe surface. Therefore, the liquid slag can not be cooled immediately when it reaches the surface of the deposition, and has sufficient time to merge with each other, so a middle layer with a relatively compact structure is formed, and the heat flux reduction rate slows down. With the increase of thickness, the overall thermal conductivity of the deposition also continues to decrease. The reason for the accelerated decline of the heat flux in the BC stage is that the growth rate of deposition at this stage. When the growth of the deposition reaches a stable stage, the deposition thickness fluctuates around a stable value. At this time, the growth rate is in dynamic balance with the erosion, melting and falling rate [15]. In the stable stage, the formation and rupture of the bubble still exist in the deposition, so the surface of the deposition has obvious pore structure, and the heat flux through the deposition fluctuates slightly in a stable range. The final stable relative heat flux is 0.585.

The heat flux through probe 2 decreases linearly in the first 21 min (OA') and remains stable and fluctuates in a small range in the following 39 min (A'D'). The rate of the decline stage is 0.0071 (1/min), which is much smaller than the initial stage of probe 1. This is because the ash in the flue gas particles are greatly reduced after the slag screen. The thickness of the deposition on probe 2 is much less than that of probe 1 in the same time interval. In addition, the size of the ash particles hitting and adhering to probe 2 is smaller than that of probe 1, so the porosity of the initial layer is smaller, and the thermal conductivity is larger, correspondingly. Combined with Fig. 4, it can be seen that the thickness of the deposits on probe 2 is thin and the accumulation is relatively tight,

which results in the final stable relative heat flux density of probe 2 is 0.850.

3.3. Microstructure of slag and deposition

Fig. 7 (I) presents the microstructure of slag (①-④) and the deposition on the windward side of probe 1. The first column is 25X magnification image, and the two columns on the right are high magnification images. It can be seen from the low magnification picture that the granulated slag presents a pore structure that is obviously different from other slag samples. The surface of the granulated slag is compact and smooth, and the pores are small and dispersed. The calculated porosity of the granulated slag is only 19.84%, which indicates that the granulated slag has a high degree of vitrification. It can be seen from the high magnification picture that some regular white crystals are attached to the surface of the granulated slag. EDS analysis shows that the mass fraction of Fe and Mg elements in the white crystal is 32.8% and 4.39%, respectively. Combined with XRD analysis, it can be inferred that this is $MgAl_{1.6}Fe_{1.4}O_4$ crystal precipitated from liquid slag during cooling process.

The remaining slag samples showed severe sintering traces, and many large-diameter pores could be observed in the picture. The porosity of the top, middle and bottom layers of the slag on the partition of the burnout chamber is 54.89%, 44.41%, and 27.30%, respectively; The porosity of the upper and bottom layers of the slag on the slag hole is 36.59% and 26.52%, respectively; The porosity of the upper and bottom

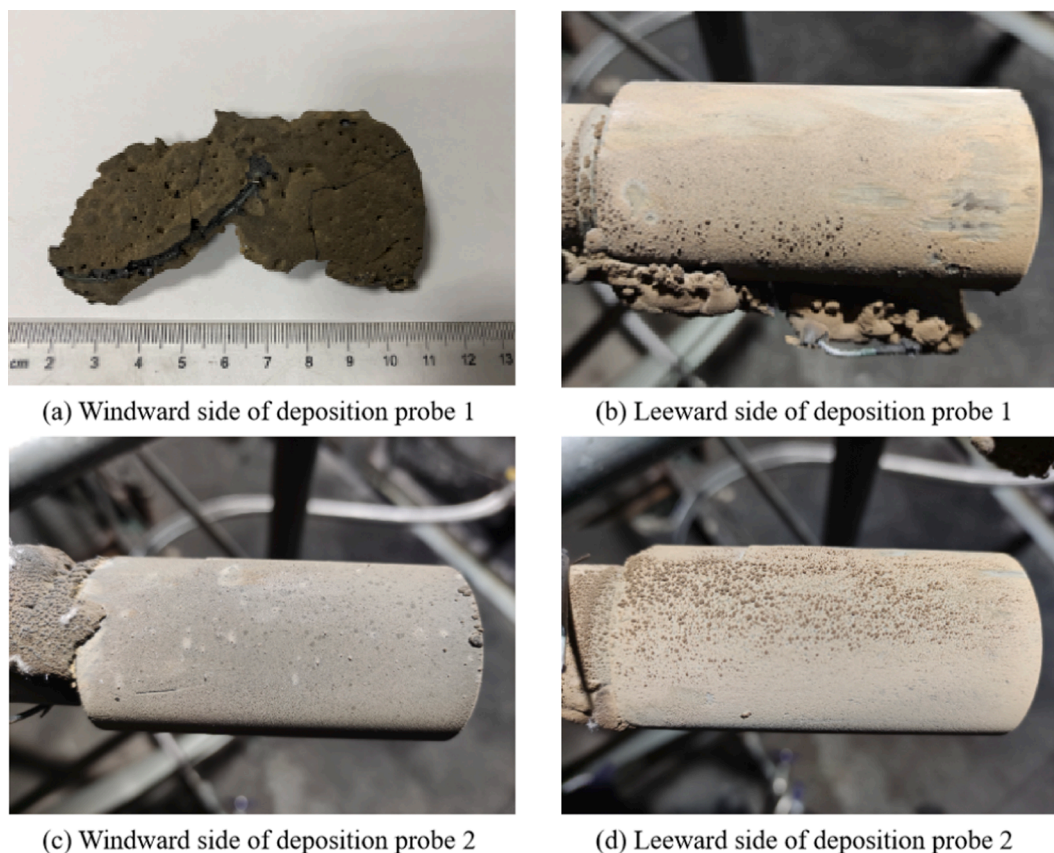


Fig. 4. The appearance of deposition on the probe.

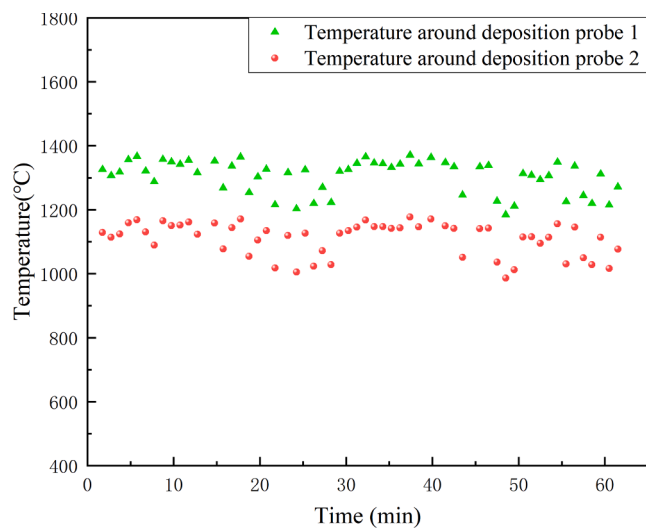


Fig. 5. Temperatures around deposition probes.

layers of the slag on the windward side of the slag screen is 34.85% and 53.14% respectively; The porosity of the deposition on the windward side of probe 1 is 36.26%. According to the high magnification image, the main mineral phases of the slag are silicates and iron-containing compounds.

Fig. 7 (II) is the microstructure of the ash sample (⑤–⑦). It can be seen from the figure that the agglomeration of the ash particles becomes less obvious with the decrease of the temperature of the sampling point. The reason is that Na, K and alkaline earth metal elements deposit preferentially on the leeward side of the slag screen and the thermostat

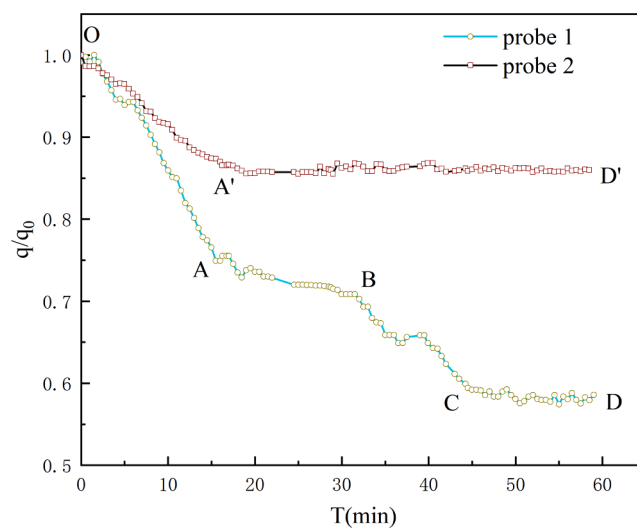


Fig. 6. Heat flux through the deposition probes versus time.

screen forming sulfate with strong adhesion. These sulfates will also adhere to the surface of the ash particles, forming flocculent aggregate particles.

3.4. Chemical composition of slag and deposition

Table 3 describes the oxide composition of slag and deposition samples collected at different locations. In order to intuitively reflect the migration characteristics of elements, the stacked plots of slag and deposition samples at different positions are drawn, as shown in Fig. 8. It

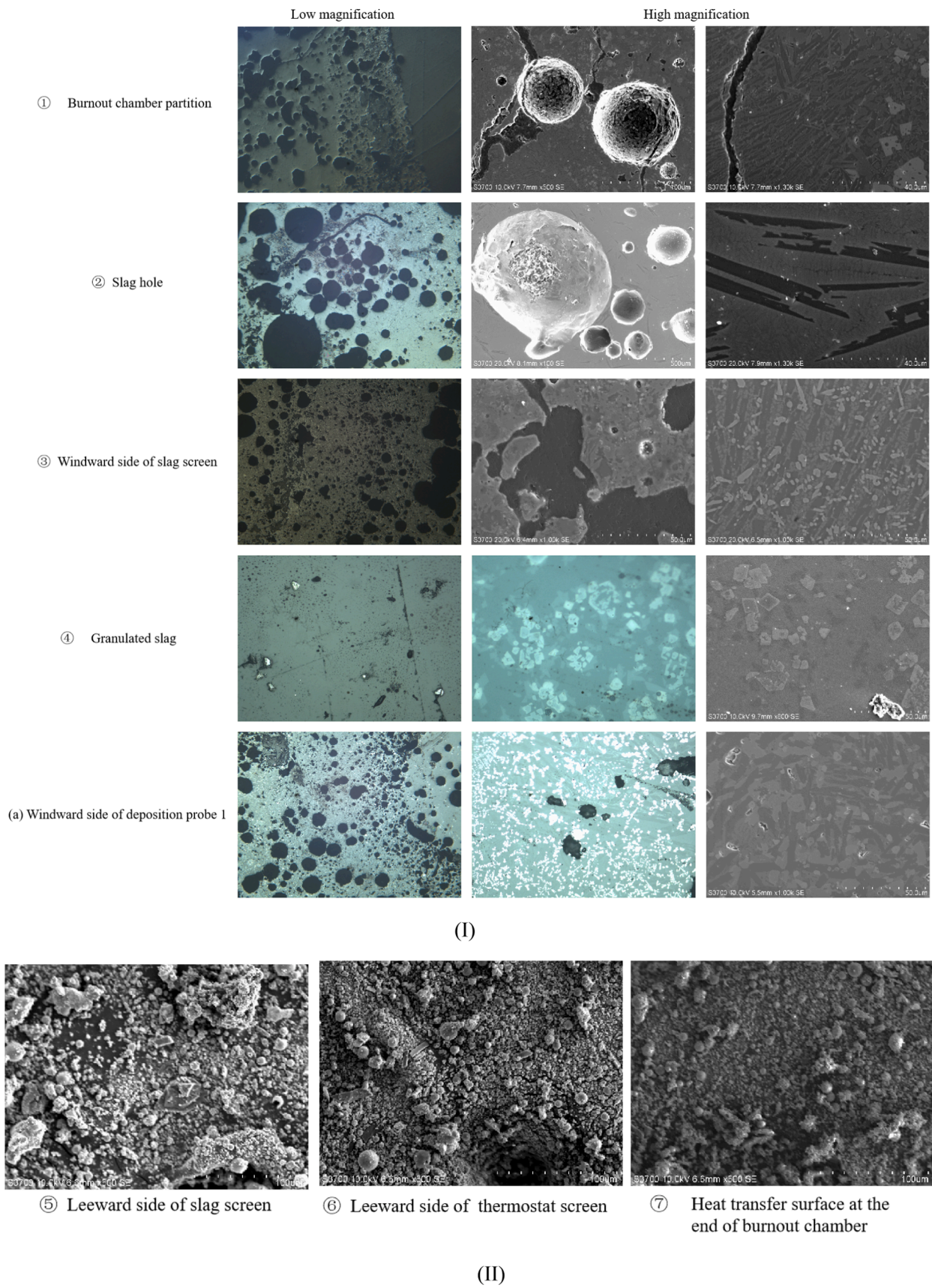


Fig. 7. The microstructure of slag and deposition.

Table 3
Chemical composition of slag and deposition

Sampling location	Al ₂ O ₃	CaO	Fe ₂ O ₃	K ₂ O	MgO	Na ₂ O	SiO ₂	SO ₃	TiO ₂	Cl
①Burnout chamber partition	16.40	14.90	32.96	0.94	2.70	1.40	27.25	0.28	1.04	/
②Slag hole	14.46	10.92	41.02	0.84	1.55	0.79	27.14	0.24	0.87	/
③Windward side of slag screen	14.98	15.39	35.35	0.90	2.76	1.81	25.46	0.30	1.08	/
④Granulated slag	13.94	15.90	37.59	0.70	2.83	0.92	24.81	0.11	0.91	/
⑤Leeward side of slag screen	14.09	18.63	24.70	2.11	4.30	5.40	19.21	6.76	0.93	0.40
⑥Leeward side of thermostat screen	13.82	20.04	23.46	2.05	4.27	5.06	19.48	7.18	0.90	0.25
⑦Heat transfer surface at the end of burnout chamber	8.93	22.18	32.20	1.08	4.93	3.17	12.71	10.45	0.63	0.29
(a) Windward side of probe 1	15.81	12.01	36.35	0.96	2.18	1.23	28.12	0.27	1.05	/
(b) Leeward side of probe 1	14.27	17.09	24.79	2.19	4.13	5.79	20.23	7.44	0.93	0.40
(c) Windward side of probe 2	10.95	15.89	38.94	1.55	3.82	4.75	13.15	7.07	1.01	0.20
(d) Leeward side of probe 2	15.12	18.75	22.13	2.26	4.08	5.26	21.98	6.60	0.94	0.31

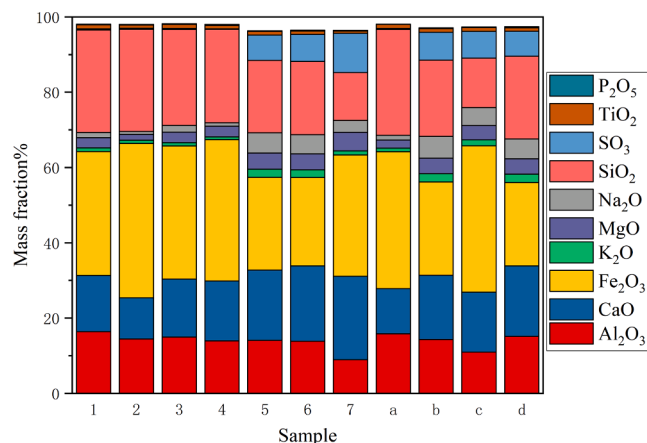


Fig. 8. Stacking diagram of oxide composition of different slag and deposition samples.

can be seen from the figure that the major components in ash and deposition samples are Al₂O₃, CaO, Fe₂O₃ and SiO₂, which account for more than 75% of the total mass. The content of Al₂O₃ in each sample is almost the same. Except for the heat transfer surface at the end of burnout chamber, the content of Al₂O₃ in the fly ash at this location is only 8.93%. The content of Na₂O in slag (①–④) is 1.40%, 0.79%, 1.81%, 0.92%, respectively. The content of Na₂O in ash (⑤–⑦) is 5.40%, 5.06%, 3.14% respectively, which is significantly higher than that in slag samples. The reason is that the temperature of ash sample is lower than that of slag sample. During the combustion of high-alkali coal, most sodium is sublimated directly into gaseous Na or released into the gas phase in the form of Na₂O and NaCl, and the remaining sodium is converted into aluminosilicate at high temperature [10]. Sodium in the gas phase has a strong tendency to deposit and is easy to condense and deposit in the range of 600–900°C [18]. The same phenomenon also occurs in the distribution of K₂O. The average concentration of K₂O in the ash sample is 1.75%, while that in slag sample is 0.84%. Interestingly, the content of Na₂O and K₂O in the ash sample on the heat transfer surface at the end of burnout chamber is less than those on the leeward side of the thermostat screen and slag screen. This distribution characteristic is due to the low temperature of heat transfer surface at the end of burnout chamber, and most of the sodium and potassium in the gas phase condenses on the heat transfer surface at the front of the furnace. Na₂O and K₂O are rarely found on the windward side of probe 1 (a), but are abundantly enriched on the leeward side of probe 1 and probe 2 (b–d). The alkali metals on the probe mainly exist in the initial layer of deposition [9]. Due to the smaller mass of the deposition of b–d, the proportion of the initial layer is larger, and the alkali metal concentration is higher than a. As alkaline oxides, MgO and CaO have similar distribution characteristics to Na₂O and K₂O. The enrichment of alkali metals in the low temperature region also leads to the

deposition of sulfur and chlorine. It can be seen from Table 3 that the presence of Cl is almost undetectable in the slag sample, and the average concentration of SO₃ is only 0.23%. In contrast, the presence of Cl is only detected in the ash samples, and the average concentration of SO₃ in the ash is as high as 8.13%. It can be speculated that there are Na₂SO₄, NaCl, KCl, CaSO₄, MgSO₄ and other compounds in the ash samples in the low temperature region of the boiler. These low melting point compounds will deposit on the heat exchange surface or adhere to the surface of the ash particles, increasing the adhesion of the ash particles.

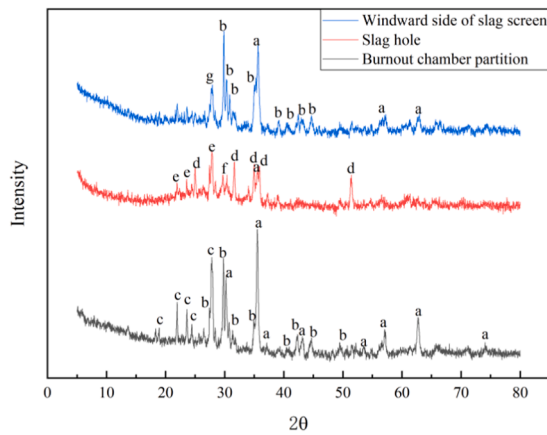
HSQ is high-alkali and rich-iron coal, so the content of Fe₂O₃ in slag and deposition samples is very high. The average concentration of Fe₂O₃ in the slag sample is 36.73%, while that in ash sample is 26.78%. The research of Wei indicates that Fe is an excellent fluxing agent for the silicon-calcium-magnesium–aluminum system, and Fe₂O₃ can reduce the melting point of ash to form low temperature eutectic [19]. This also explains why the content of Fe₂O₃ in slag sample is higher than that in ash sample.

3.5. Mineralogy of slag and deposition

In order to further understand the characteristics and mechanism of element migration during the combustion of HSQ, XRD is used to analyze the composition of major crystalline compounds in slag and deposition samples at various locations. The processed analysis curve is shown in Fig. 9.

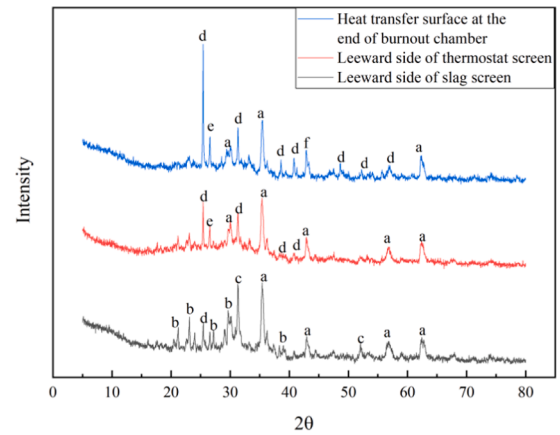
The slag at the partition of the burnout chamber is mainly composed of magnesioferrite (MgFe₂O₄), augite ((CaMg_{0.74}Fe_{0.25})Si₂O₆) and andesine (Na_{0.685}Ca_{0.347}Al_{1.46}Si_{2.54}O₈). The slag sample at the slag hole is mainly composed of fayalite (Fe₂SiO₄), bytownite (Ca_{0.86}Na_{0.14}Al_{1.9}Si_{2.06}O₈), diopside (CaMgSi₂O₆) and a small amount of magnesioferrite. The slag sample on the windward side of the slag screen is mainly composed of magnesioferrite, augite and ferrosilite magnesian (Mg_{0.93}Fe_{1.07}Si₂O₆). It can be found that the crystal phase of slag sample is mainly composed of silicate and iron-magnesium compounds. This is consistent with the composition in Table 3, Fe₂O₃ and SiO₂ occupy more than 60% of the oxide composition of the slag sample. Part of the calcium, sodium and magnesium compounds decomposed at high temperature will react with SiO₂ to form silicate, so the slag sample will contain a small amount of insoluble calcium, sodium and magnesium [11]. The formation of low-temperature eutectics such as magnesioferrite and fayalite reduces the melting point of ash, while the increase in the ratio of iron to calcium inhibits the formation of high melting point mullite [20]. With the increase of temperature, augite will transform into peridot and melilite, resulting in the intensification of eutectic reaction and the decrease of ash melting temperature [21].

As shown in Fig. 9 (II), the ash on the leeward side of the slag screen is mainly composed of magnesium iron oxide (Mg_{1.55}Fe_{1.6}O₄), nepheline (K_{0.48}Na_{3.48}(Al_{0.99}Si_{1.01}O₄)₄), and gehlenite (Ca₂(Al(AlSi)O₇)). The crystal composition of the ash on the leeward side of the thermostat screen is similar to that of the ash on heat transfer surface at the end of burnout chamber, which is mainly composed of oxides and sulfates such as



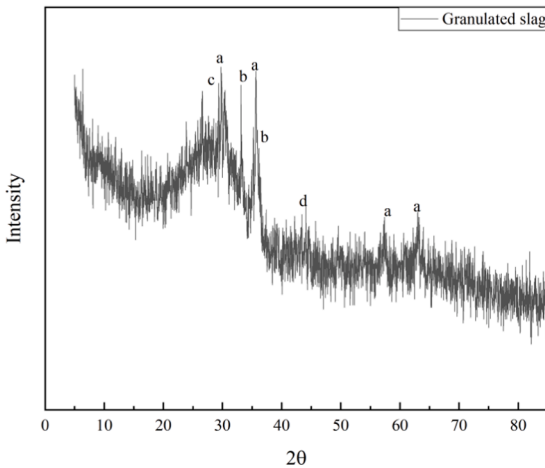
a: MgFe_2O_4 (Magnesioferrite); b: $(\text{CaMg}_{0.74}\text{Fe}_{0.25})\text{Si}_2\text{O}_6$ (Augite);
 c: $\text{Na}_{0.685}\text{Ca}_{0.347}\text{Al}_{1.46}\text{Si}_{2.54}\text{O}_8$ (Andesine); d: Fe_2SiO_4 (Fayalite);
 e: $\text{Ca}_{0.86}\text{Na}_{0.14}\text{Al}_{1.9}\text{Si}_{2.06}\text{O}_8$ (Bytownite); f: $\text{CaMgSi}_2\text{O}_6$ (Diopside);
 g: $\text{Mg}_{0.93}\text{Fe}_{1.07}\text{Si}_2\text{O}_6$ (Ferrosilite magnesian)

(I)



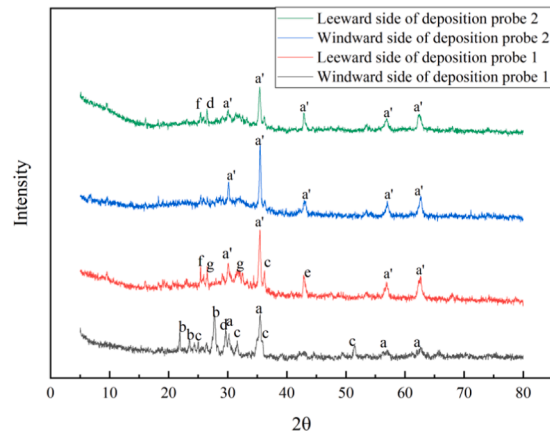
a: $\text{Mg}_{1.55}\text{Fe}_{1.6}\text{O}_4$ (Magnesium Iron Oxide); b: $\text{K}_{0.48}\text{Na}_{3.48}(\text{Al}_{0.99}\text{Si}_{1.01}\text{O}_4)_4$ (Nepheline);
 c: $\text{Ca}_2(\text{Al}(\text{AlSi})\text{O}_7)$ (Gehlenite); d: CaSO_4 (Anhydrite); e: SiO_2 ; f: MgO

(II)



a: $\text{MgAl}_{1.6}\text{Fe}_{1.4}\text{O}_4$ (Magnesium Aluminum Iron Oxide); b: $\text{Ca}_3\text{Fe}_2(\text{SiO}_4)_3$ (Andradite);
 c: $(\text{Mg}_{0.944}\text{Fe}_{0.056})(\text{Ca}_{0.844}\text{Na}_{0.14}\text{Fe}_{0.014})(\text{Si}_{1.86}\text{Al}_{0.14}\text{O}_6)$ (Diopside aluminian); d: CaSi_2

(III)



a: MgFe_2O_4 (Magnesioferrite); a': $\text{Mg}_{1.55}\text{Fe}_{1.6}\text{O}_4$ (Magnesium Iron Oxide);
 b: $\text{Ca}_{0.65}\text{Na}_{0.32}\text{Al}_{1.62}\text{Si}_{2.38}\text{O}_8$ (Labradorite); c: Fe_2SiO_4 (Fayalite);
 d: SiO_2 ; e: MgO; f: CaSO_4 (Anhydrite)

(IV)

Fig. 9. XRD analysis of slag and deposition.

$\text{Mg}_{1.55}\text{Fe}_{1.6}\text{O}_4$, anhydrite (CaSO_4), quartz and MgO. This result is consistent with the conclusion in Section 2.4 that alkali metal elements such as Na, K, Mg, and Ca will be enriched in the fly ash in the low temperature region and react with SO_3 to form sulfate. According to Wang's research, Sodium element mainly exists in the form of aluminosilicate and sulfide crystals in low temperature area [8]. However, in this study, Na was only found in nepheline, while sulfur is mainly found in CaSO_4 , which may be related to the enrichment of Ca in the low temperature region.

Fig. 9 (III) shows the XRD analysis curve of the granulated slag collected by the slag conveyor. It can be seen that the curve fluctuates greatly and is not as smooth as other samples, indicating that the granulated slag has a lower degree of crystallinity and is closer to glassy slag. The conclusion given in the research of Chen [14] shows that the liquid slag with a high Si/Al ratio has a low crystallization tendency, and the viscosity increases gradually with the decrease of temperature, which is closer to the characteristics of glassy slag. The increase of Na_2O and CaO will increase the possibility of crystallization. The major crystal phases in the granulated slag are $\text{MgAl}_{1.6}\text{Fe}_{1.4}\text{O}_4$, andradite ($\text{Ca}_3\text{Fe}_2(\text{SiO}_4)_3$), Diopside aluminian ($(\text{Mg}_{0.944}\text{Fe}_{0.056})(\text{Ca}_{0.844}\text{Na}_{0.14}\text{Fe}_{0.014})(\text{Si}_{1.86}\text{Al}_{0.14}\text{O}_6)$), and CaSi_2 .

Fig. 9 (IV) is the XRD analysis spectrum of the deposition collected on the probe. The deposition on the windward surface of probe 1 is mainly composed of magnesioferrite, Labradorite ($\text{Ca}_{0.65}\text{Na}_{0.32}\text{Al}_{1.62}\text{Si}_{2.38}\text{O}_8$), fayalite and quartz. The deposition on the leeward side of probe 1 is mainly composed of $\text{Mg}_{1.55}\text{Fe}_{1.6}\text{O}_4$, fayalite, MgO and anhydrite. The main crystal phases of the deposition on probe 2 are $\text{Mg}_{1.55}\text{Fe}_{1.6}\text{O}_4$, quartz and anhydrite. The crystal phases in the high temperature zone are complexes, in which iron is enriched, while calcium and sulfur are enriched in the low temperature region, and the crystal phase is dominated by oxides and sulfates. According to the above XRD analysis, the formation of low melting point compounds and the condensation of vapor alkali metals are the main reasons for ash deposition on high temperature and low temperature heat exchange surface respectively.

4. Conclusions

In this work HSQ is burned in a 20 MW liquid slagging cyclone furnace. The characteristics of element migration and ash deposition are examined. In addition, the microscopic morphology, crystal structure and chemical composition of the slag are studied to explain the effect of element migration on ash deposition and slag.

1. The growth process of deposition on the probe in front of the slag screen can be divided into four stages, the durations of each stage are 18, 13, 15 and 14 mins, while the decline rates of relative heat flow are 0.0147, 0.00208, 0.0082 and 0 (1/min), respectively. The final stable relative heat flux is 0.585. The heat flux through probe 2 decreases linearly in the first 21 min and remains stable and fluctuates in a small range in the following 39 min, the final stable relative heat flux is 0.850.
2. Na, K, Ca, Mg and S are enriched in the low temperature area of the boiler to form sulfate with strong adhesion. These sulfates will also adhere to the surface of the ash particles, forming flocculent aggregate particles.
3. The main mineral phases of the slag are silicates and iron-containing compounds. Iron will be enriched in the slag and form a low-temperature eutectic with the silicon-calcium-magnesium-aluminum system to reduce the melting point of the ash.
4. The granulated slag has a lower degree of crystallinity and is closer to the characteristics of glassy slag, which is due to the low content of Na_2O , CaO and high silicon-to-aluminum ratio in the ash.

Declaration of Competing Interest

The authors declare that they have no known competing financial interests or personal relationships that could have appeared to influence the work reported in this paper.

Acknowledgement

This work was supported by National Natural Science Foundation of China (52036008).

References

- [1] Guo X, Zhang H, Zhu Z. The effect of O_2/C ratio on gasification performance and sodium transformation of Zhundong coal. *Fuel Process Technol* 2019;193:31–8.
- [2] Qi X, Song G, Yang S, Yang Z, Lyu Q. Migration and transformation of sodium and chlorine in high-sodium high-chlorine Xinjiang lignite during circulating fluidized bed combustion. *J Energy Inst* 2019;92(3):673–81.
- [3] Xu L, Kang Y, Zhang G, Wang T, Wu T. Study of alkali emission and control with firing a high alkali coal. *Combust Sci Technol* 2015;187(12):1959–73.
- [4] Shen Z, Hua X, Liang Q, Xu JianLiang, Han D, Liu H. Reaction, crystallization and element migration in coal slag melt during isothermal molten process. *Fuel* 2017; 191:221–9.
- [5] Ishiga T, Kiso F, Suetsugu A, Utano M, Yamashita H, Ueki Y, et al. Heating technique of slag-tapping hole in high-temperature coal gasifier. *Fuel Process Technol* 2015;138:100–8.
- [6] Zhang H, Guo X, Zhu Z. Effect of temperature on gasification performance and sodium transformation of Zhundong coal. *Fuel* 2017;189:301–11.
- [7] Li X, Li J, Wu G-G, Bai Z-Q, Li W. Clean and efficient utilization of sodium-rich Zhundong coals in China: behaviors of sodium species during thermal conversion processes. *Fuel* 2018;218:162–73.
- [8] Wang C, Li G, Du Y, Yan Yu, Li H, Che D. Ash deposition and sodium migration behaviors during combustion of Zhundong coals in a drop tube furnace. *J Energy Inst* 2018;91(2):251–61.
- [9] Li G, Wang C, Wang P, Du Y, Liu X, Chen W, et al. Ash deposition and alkali metal migration during Zhundong high-alkali coal gasification. *Energy Procedia* 2017; 105:1350–5.
- [10] Li G, Wang C, Yan Yu, Jin Xi, Liu Y, Che D. Release and transformation of sodium during combustion of Zhundong coals. *J Energy Inst* 2016;89(1):48–56.
- [11] Liang D, Xie Q, Wei Z, Wan C, Li G, Cao J. Transformation of alkali and alkaline earth metals in Zhundong coal during pyrolysis in an entrained flow bed reactor. *J Anal Appl Pyrol* 2019;142:104661. <https://doi.org/10.1016/j.jaap.2019.104661>.
- [12] Yu K, Chen X, Cai T, Ma J, Liu D, Liang C. Release and migration characteristics of sodium and potassium in high alkali coal under oxy-fuel fluidized bed combustion condition. *Fuel* 2020;262:116413. <https://doi.org/10.1016/j.fuel.2019.116413>.
- [13] Wang C, Zhao L, Sun R, Hu Y, Tang G, Chen W, et al. Effects of silicon-aluminum additives on ash mineralogy, morphology, and transformation of sodium, calcium, and iron during oxy-fuel combustion of Zhundong high-alkali coal. *Int J Greenhouse Gas Control* 2019;91:102832. <https://doi.org/10.1016/j.ijggc.2019.102832>.
- [14] Chen X, Kong L, Bai J, Dai X, Li H, Bai Z, et al. The key for sodium-rich coal utilization in entrained flow gasifier: the role of sodium on slag viscosity-temperature behavior at high temperatures. *Appl Energy* 2017;206:1241–9.
- [15] Zhou H, Zhou B, Li L, Zhang H. Experimental measurement of the effective thermal conductivity of ash deposit for high sodium coal (Zhundong coal) in a 300 kW test furnace. *Energy Fuels* 2013;27(11):7008–22.
- [16] Song W, Tang L, Zhu X, Wu Y, Zhu Z, Koyama S. Flow properties and rheology of slag from coal gasification. *Fuel* 2010;89(7):1709–15.
- [17] Zhou H, Zhou B, Dong K, Ding J, Cen K. Research on the slagging characteristics of easy to slagging coal in a pilot scale furnace. *Fuel* 2013;109:608–15.
- [18] Lei Y, Fu P, Tang S, Yue F, Bie K, Liu Y. Occurrence form of sodium in Zhundong coal and its evaporation and condensation characteristics. *Journal of Combust Sci Technol* 2019;25(02):124–30 (in Chinese).
- [19] Wei B, Tan H, Wang X, Ruan R, Hu Z, Wang Y. Effect of Na/Ca/Fe on slagging behavior of Zhundong coal during combustion process. *J Chinese Soc Power Eng* 2017;37:685–90.
- [20] Zhou S, Wang M, Tan H, Wang X, Yang W, Xiong X, et al. Evaluation of aluminum ash in alleviating the ash deposition of high-sodium and high-iron coal. *Fuel* 2020; 273:117701. <https://doi.org/10.1016/j.fuel.2020.117701>.
- [21] Li L, Wang Y, Wang M, Zhou S, Tan H. Experiment of adding $\text{Ca}_3(\text{PO}_4)_2$ to alleviate slagging of high sodium rich iron blended coal. *Thermal Powergeneration*. 2021: 1–10.